Volume 2
Number 5
September 2025
Pages 619–774

RSC Mechanochemistry

rsc.li/RSCMechanochem

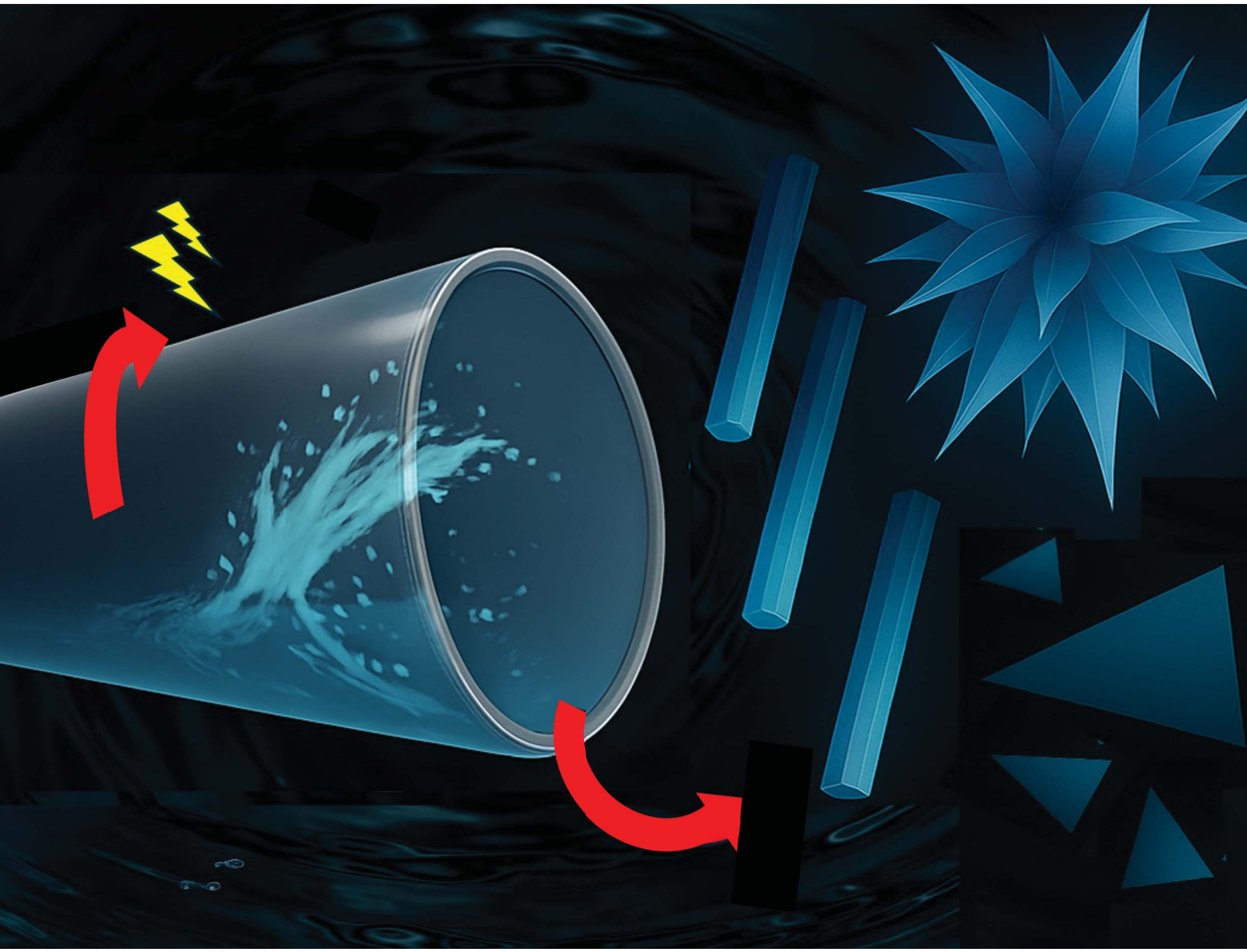

ISSN 2976-8683

ROYAL SOCIETY OF CHEMISTRY

PAPER
Badriah M. Alotaibi *et al.*
Aqueous photo-induced high shear shape selective pristine silver nano/micro particles

RSC Mechanochemistry

ROYAL SOCIETY OF CHEMISTRY

PAPER

View Article Online
View Journal | View Issue

Cite this: *RSC Mechanochem.*, 2025, **2**, 653

Aqueous photo-induced high shear shape selective pristine silver nano/micro particles†

Badriah M. Alotaibi,[a] Chengyi Liu,[b] Xianjue Chen[b] and Colin L. Raston *[a]

Received 16th January 2025
Accepted 15th July 2025

DOI: 10.1039/d5mr00013k

rsc.li/RSCMechanochem

We report an efficient photo-contact electrification (CE) method for controlling the synthesis of pristine silver nanoparticles of different shapes, as one, two, and three-dimensional materials, notably rods, spicules and triangles. This uses a vortex fluidic device (VFD) which houses a rapidly rotating quartz tube tilted at 45° while the aqueous silver nitrate thin film is irradiated at 254 nm. The photo-CE associated with the mechanical energy imparted into the liquid in the microfluidic platform allows control of the size and shape of the nanoparticles, and some micron size particles, depending on the rotational speed of the tube and concentration of silver nitrate. Uniform shapes are generated with pristine surfaces in the absence of added reducing agents, with processing scalability under continuous flow. This synthetic method is also simple and cost-effective, and overall adheres to the principles of green chemistry.

Introduction

While gold nanoparticles have long featured in various applications, the potential of the same group silver nanoparticles is also promising.[1–3] Elemental silver stands out as an attractive metal for targeted nanoparticle synthesis due to its exceptional properties such as malleability, conductivity, chemical resistance, and antimicrobial characteristics. Silver nanoparticles (AgNPs) are versatile, having applications in catalysis, optics, medicine, water disinfection and energy storage.[2,3] Within the realms of biological impact, the antimicrobial activity of AgNPs arises from cell membrane damage and disruption of intracellular metabolic processes.[4,5] Nano-silver structures encompassing cubes, platelets, rods, spheres, triangles, and flowers, have shape specific properties.[6,7] The synthesis and growth of AgNPs into desired shapes can be achieved through the use of template assisted methods, seed-mediated growth, photochemical routes, electrochemical deposition, solvent engineering, surface functionalization, lithography techniques,[8] using polyols,[9] citric acid reduction,[10] biosynthesis[11] and using emulsions.[9,12] These methods invariably require high reaction temperature and the use of toxic solvents and stabilizing agents. In addition, a new method for rapidly synthesizing silver nanoparticles using water in a supercritical carbon dioxide emulsion has been established. Interestingly adding water droplets to the emulsion greatly improves control over nanoparticle size and their rate of formation.[13] This method involves the use of shape-directing agents[8] such as cetyltrimethylammonium bromide (CTAB) while stabilizing silver nano-particle seeds with citrate, and reducing agents. However, challenges remain for the synthesis of silver nanoparticles while maintaining purity, minimizing environmental impact of the process, including avoiding the use of waste generating excipients, avoiding the use of high temperatures and pressures, and improving the scalability of the processing.

In the present study, we introduce a new method utilizing high shear mechanical energy and associated photo-contact electrification (CE) to synthesize assemblies of nano/micro-Ag structures in water in high yield, with well-defined structures, as rods, spicules and triangles. This involves the use of a vortex fluidic device (VFD), which results in unparalleled control over the size and shape of particles within dynamic thin films of water, presenting new avenues for effectively manipulating nano-silver particles. The VFD is a thin film microfluidic platform[14] with a diverse range of applications, including the manipulation of carbon nano-materials, for example slicing carbon nanotubes,[15] exfoliating graphene and boron nitride,[16] scrolling of preformed graphene oxide[17] and graphene directly from graphite,[18] synthesizing carbon dots,[19] and assembling C_{60} into tubules.[20] More recent is the direct transformation of micron size antimony particles into few layered antimonene by an *in situ* melt and recrystallisation process.[21] Other applications of the VFD include promoting enzymatic reactions,[22] regulating chemical reactivity and selectivity,[23] and facilitating protein folding.[24] The VFD imparts high shear in a dynamic thin film in the device for which there have been advances in understanding the nature of the induced mechanical energy.[25] This is important in further advancing the applications of the device, as in the present study.

[a]*Flinders Institute for Nanoscale Science and Technology, College of Science and Engineering, Flinders University, Adelaide, SA 5042, Australia. E-mail: colin.raston@flinders.edu.au*

[b]*School of Environmental and Life Sciences, The University of Newcastle, Callaghan, New South Wales, 2308, Australia*

† Electronic supplementary information (ESI) available: Characterisation by SEM, EDX, TEM, AFM and XPS. See DOI: https://doi.org/10.1039/d5mr00013k

The VFD allows developing the use of continuous flow processing as a strategy for addressing scalability of the processing at the inception of the science,[14] with the added benefit of simplicity of operation of the relatively inexpensive microfluidic platform and its proven capability for fabricating nanomaterials in general.[26] The VFD houses a rapidly rotating tube, typically made of quartz, 20 mm in outside diameter, and 18.5 cm in length. It is usually spun up to 9000 rpm with its tilt angle, θ, set at 45° relative to the horizontal position, as shown in Fig. 1(a), noting that this angle is optimal for most applications of the device. In the continuous flow mode of operation of the VFD, jet feeds are used to deliver liquid at a controlled flow rate at different (and optionally multiple) points along its length as well as at the base of the tube, which is mostly hemispherical in shape, for the present research. The liquid then generates a thin film as it moves up the tube and exits at the top. The mechanical

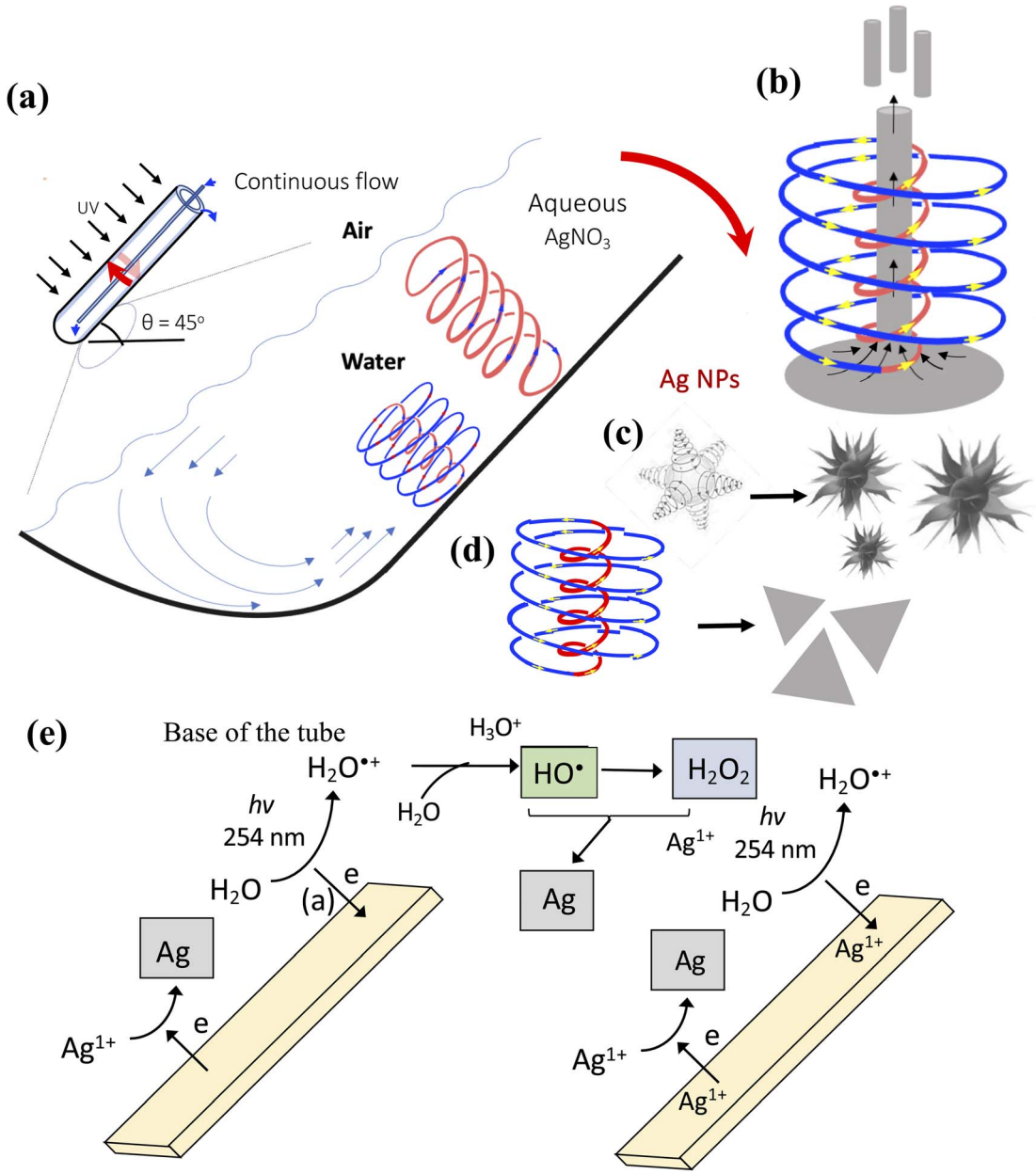

Fig. 1 (a) Schematic of the continuous flow mode of operation of the vortex fluidic device (VFD), forming (i) typhoon like spinning top (ST) topological fluid flow from the Coriolis force at the hemispherical base of the rapidly rotating quartz tube, and (ii) double helical (DH) flow from the induced Faraday wave eddies coupled with the Coriolis force from the curved surface of the tube.[14] (b) Formation of silver particles with rod structures by the uplift of the ST flow upon irradiation of the tube ($\lambda = 254$ nm). (c) and (d) Formation of spicules and triangular structures. (e) UV induced formation of silver nano/micro-structures on the surface of the quartz VFD tube with a proposed mechanism involving photo-CE induced oxidation of water to $H^{\bullet}$ and $OH^{\bullet}$. All processing outcomes are for $\theta = 45°$ using silver nitrate in water under UV irradiation, $\lambda = 254$ nm, at room temperature.

energy in the liquid is in the form of high shear topological fluid flows down to ~150 nm in diameter, as double helical (DH) flow arising from Faraday waves and side wall Coriolis force, and spinning top (ST, typhoon like) from the Coriolis force from the hemispherical base of the tube.[25] The liquid in the VFD is beyond diffusion control limits with high mass transfer, as well as high heat transfer, with the thin film facilitating uniform processing when irradiated with external light sources. We hypothesised that these unique effects in the VFD can accelerate and control the formation of silver nano-structures (Fig. 1), having recently established that pristine gold nanoparticles can be generated in auric acid when the tube is irradiated at 254 nm by a photo-CE effect.[27] The selective formation of silver rods, spicules or triangles under such UV irradiation is without the need for adding a reducing agent, or capping agents, and as such the methodology is high in green chemistry metrics. Rotational speeds of 3, 5, and 7k rpm were chosen as representatives of the impact of the different topological fluid flows. At 3 and 5k rpm, the fluid flow is dominated by ST flow whereas for 7k rpm it is dominated by DH and spicular flows.

Results and discussion

Ag particles with nano/micro-structures were readily prepared in high yield (70–80%) in an aqueous silver nitrate solution of different concentrations, while the rotating tube in the VFD was spun at different speeds under irradiation (254 nm), as shown in Fig. 1(a)–(d) and S1.† Auric acid can be reduced under such conditions for which we established a photo-CE process. This likely leads to the formation of silver particles with the oxidation of water coupled with the reduction of silver ions on the surface of the quartz tube, as presented in Fig. 1(c). The process involves oxidation of water to $H_2O^{\bullet+}$ and reduction of Ag^+, with such reduction also possible from the hydroxyl radical, $OH^\bullet$ derived from the loss of H^+ from $H_2O^{\bullet+}$, and the superoxide radical anion $O^{2\bullet-}$ which is associated with oxidation of water alone in the VFD under photo-CE.

Initially, we systematically investigated the formation of silver particles using a VFD operating in the confined mode, exploring various processing parameters, notably rotational speed (3, 5 and 7k rpm) and reaction time (10, 20 and 30 minutes), along with concentration of silver nitrate set at 0.5 mg mL^{-1} (0.003 M). The focus was on understanding the impact of these parameters on the formation of elemental silver for translation into continuous flow processing for scaling up purposes, which is a well-established strategy for VFD processing in general.[14,28] Processing the clear aqueous $AgNO_3$ solutions within the VFD while the quartz tube was irradiated with UV light at 245 nm (20 W), resulted in the rapid formation of a grey solution for all experiments, as shown in Fig. S1.† This is consistent with the formation of silver particles, which was confirmed using a number of techniques (see below). The formation of elemental silver is associated with the pH of the solution decreasing from 3 to 2 after VFD processing.

Three remarkably different silver structures are formed in the VFD, depending on the processing time, all being of uniform size and morphology as established using SEM. Processing at 3k rpm for 10 min resulted in only 50% of rods being formed, transitioning to 10% flower structures after 20 min, and forming 80% rods after 30 min, as shown in Fig. S2.† Increasing the speed to 5k rpm resulted in 80% yield of well-defined uniform rods over just 10 min, as shown in Fig. 2(a). The rods have a size distribution of ~200 nm (approximate range 200 nm to 3 μm) which is consistent with their formation being within the confines of the DH flow, as shown in Fig. 2(b), noting a similar structure for the shear stress induced crystallisation of fullerene C_{60}.[14] Rods also persisted after 20 min processing, as shown in Fig. S3,† but after 30 min, small particles of silver become evident along with some sheet structures, as shown in Fig. S3.†

Further increasing the rotational speed to 7k rpm resulted in the formation of rods as 80% of the product within 10 min, as shown in Fig. S4.† Extending the processing time to 20 min resulted in the rod structures being transformed into spicule structures, having a size distribution of ~3.5 μm (approximate range 2.5 to 4.5 μm) as shown in Fig. 3(a) and (b). This is unexpected but we note that the aforementioned high shear ST and DH flows create transient submicron localised temperatures exceeding the melting point of bismuth, mp 271.4 °C,[14] and also that of antimony which has a much higher melting point of 630.6 °C.[28] Here micron size spheroidal particles of the metalloid are transformed in the VFD into 2D antimonene a few layers thick.[21] The formation of high shear regimes in the VFD is related to the cavitation process, with the advantage that the high shear is delivered in a controlled way in the VFD. Cavitation in water can lead to localised temperatures in excess of several thousand Kelvin[29] and given the nexus with high shear regimes in the VFD and the reforming of the silver rods to spicules in the device, silver, which has a melting point of 961 °C, is possibly undergoing such a melting and recrystallisation. The resulting spicules take on the shape of the dominant high shear/high temperature topological fluid flow within the VFD, as previously highlighted by spicules of C_{60} of uniform size and shape also being formed in the VFD, by a shear stress induced crystallisation process.[14] An alternative process is oxidation of the silver rods followed by reduction through *in situ* generated hydrogen peroxide and possibly hydrogen (see below).

Increasing the concentration of silver nitrate to 2 mg mL^{-1} (0.01 M) resulted in the formation of triangular prisms of silver for 7k rpm and 10 min processing time, as shown in Fig. 4(a), with a size distribution of ~50 nm (approximate range 40 to 100 nm), as shown in Fig. 4(b). The formation of flat sheets of silver is consistent with the effect of the high shear on the surface of the tube being impacted by the ST topological fluid flow, as shown in Fig. 1(d). The different outcome associated with changing the concentration is consistent with the topological fluid flows being impacted by the ion activity of the solution by NO_3^- ions and Ag^+/H_3O^+ ions, with the depleted silver ions being replaced by hydronium ions, which is reflected in the change in pH (see below).

The size, shape, structure, and elemental composition of the rods, spicules, and triangles were investigated using transmission electron microscopy (TEM), as shown in Fig. 2(c), 3(c) and 4(c). TEM images revealed well-defined crystalline particles,

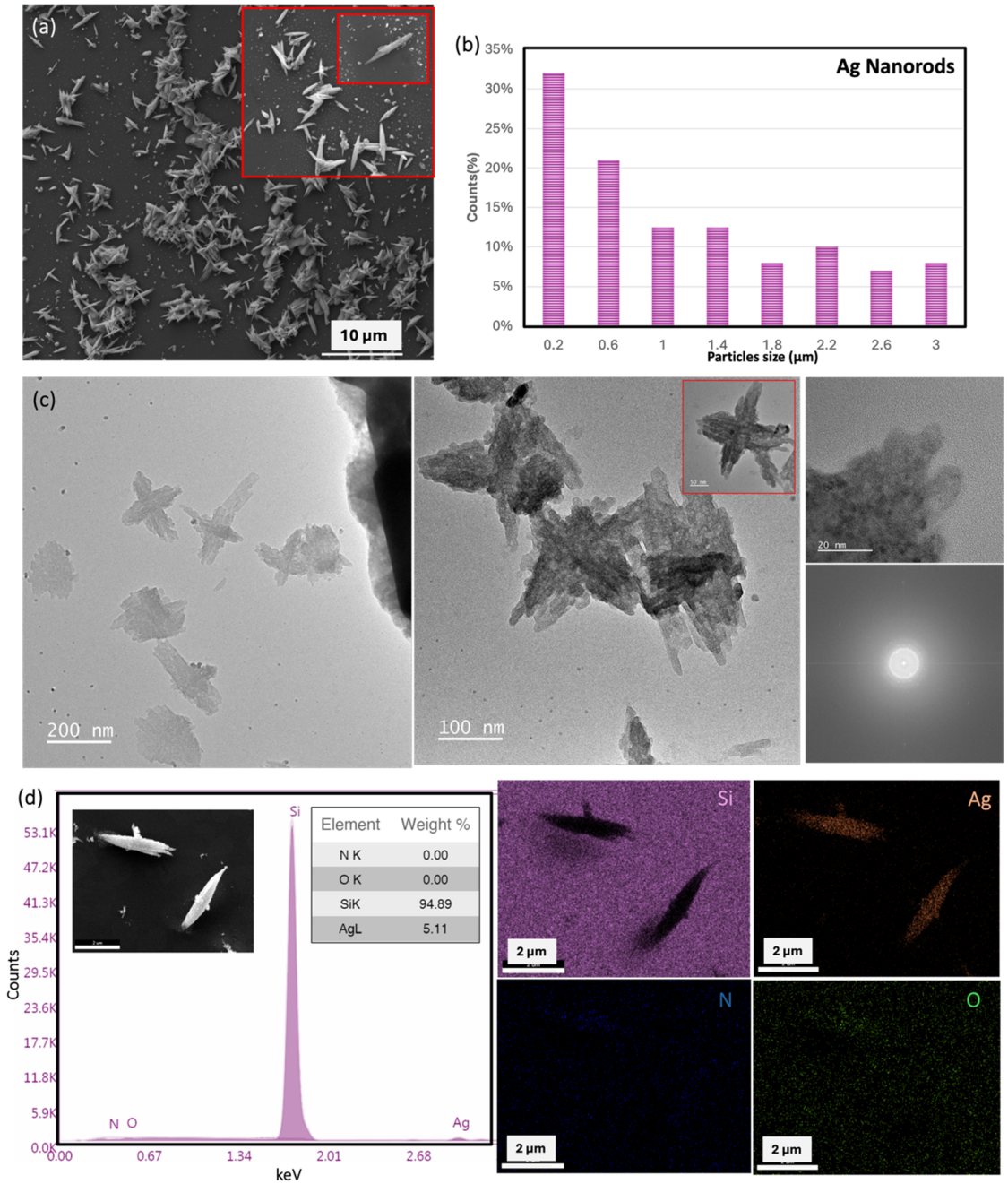

Fig. 2 (a) SEM images of silver rods, (b) particle size distribution of the rods, in (a), and (c) TEM/HRTEM image and related Fast Fourier Transform (FFT) pattern. (d) EDX spectra and elemental mapping for Ag, N, O, and Si. The VFD processing conditions are as follows: (a) ω = 5k rpm, t = 10 min, c = 0.003 M (0.5 mg per mL H_2O), θ = 45°, λ = 254 nm.

with lattice fringes corresponding to the *d*-spacing (0.23 nm) which is characteristic of face-centred cubic (FCC) Ag, as shown in Fig. 2(c), 3(c) and 4(c). It was observed that the Ag triangles are slightly affected when using a high voltage (200 kV) beam under TEM, compared to a SEM operating at 10 kV. Energy-dispersive X-ray (EDX) elemental mapping confirms the presence of silver throughout the particles, with a uniform distribution for elemental Ag with no O or N present, in accordance with the formation of elemental silver, as shown in Fig. 2(d), 3(d) and 4(d). The Ag triangles were studied using atomic force microscopy (AFM), as shown in Fig. 4(e), with an approximate height (thickness of the triangles) of ~24 nm. X-ray photoelectron spectroscopy (XPS) of the rod structures shows peaks with binding energies of 368.30 eV and 374.31 eV, corresponding to the $3d_{5/2}$ and $3d_{3/2}$ orbitals of Ag(0), as shown in Fig. 5, which is consistent with the previous literature findings related to silver particles.[30]

We have developed a comprehensive set of parameters for the formation of three distinct silver nanoparticle shapes, optimized through variation in concentration and rotational

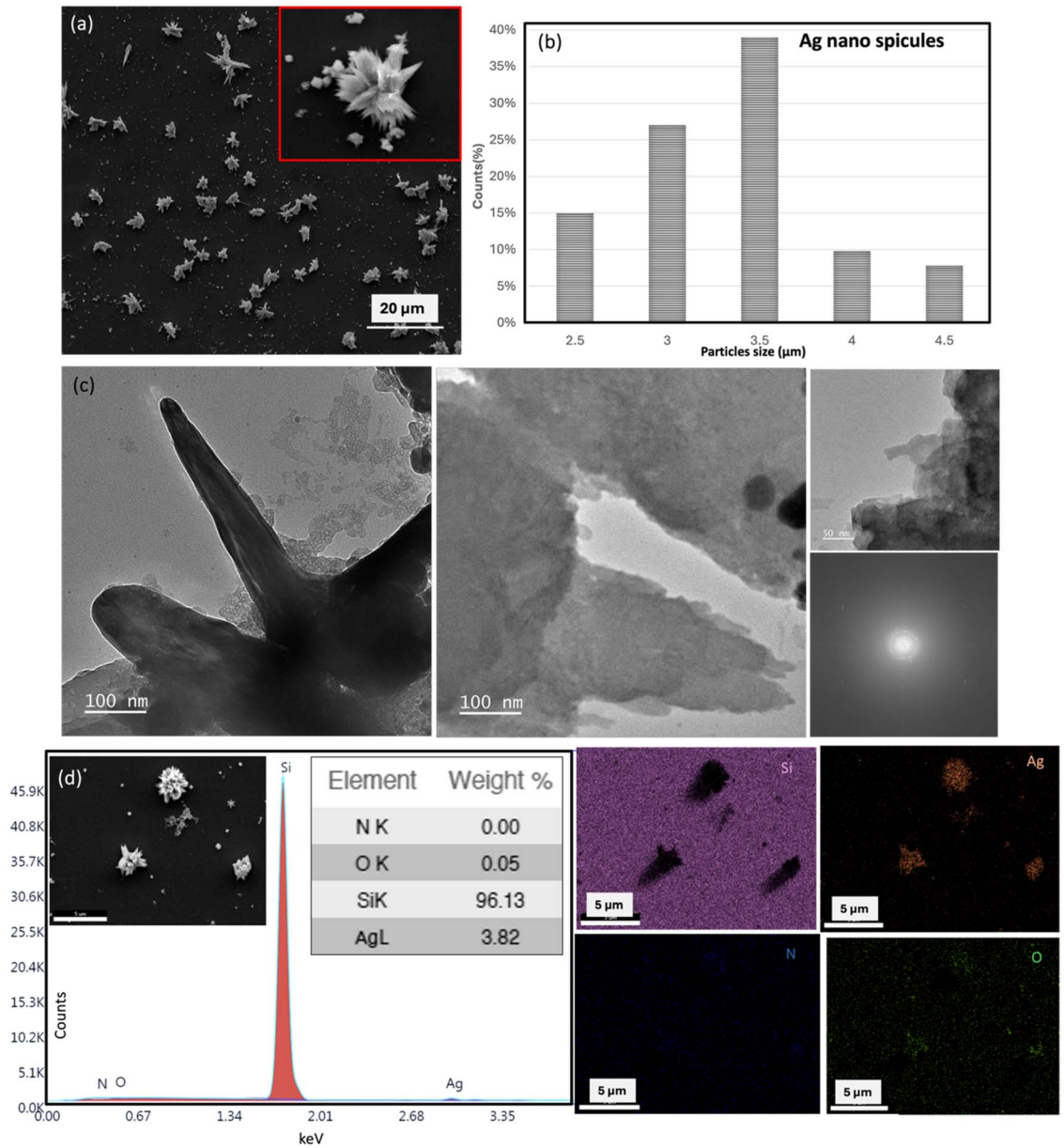

Fig. 3 (a) SEM images of spicule structures of silver, (b) particle size distribution, (c) TEM/HRTEM image and related FFT pattern, and (d) EDX spectra and elemental mapping for Ag, N, O, and Si. VFD processing conditions are as follows: $\omega = 7$k rpm, $t = 20$ min, $c = 0.003$ M (0.5 mg per mL H_2O), $\theta = 45°$, $\lambda = 254$ nm.

speed, facilitated by the *in situ* generation of hydrogen peroxide (H_2O_2) as a reducing agent or the hydroxyl radical precursor during the photo-CE process in the VFD. H_2O_2 can be both an oxidizing and reducing agent;[31] reactions such as the oxidation of silver by H_2O_2 ($\Delta E^{\circ} = +0.964$ V) and the reduction of silver ions by H_2O_2 ($\Delta E^{\circ} = +0.104$ V) can both occur. The mechanism possibly involves H_2O_2 oxidizing AgNPs to silver ions while simultaneously reducing these ions back to metallic silver, thereby facilitating the growth of AgNPs.[31] This work required specific conditions including low concentrations of H_2O_2 to minimize oxidative dissolution and pH of the solution. In the present study we have established the ability to control the formation of silver nanoparticle with controlled shape formation by the *in situ* generated H_2O_2 as an oxidizing and reducing agent, and as a shape-controlling agent. While hydrogen is generated through photo-contact electrification, a control experiment conducted for a 0.01 M $AgNO_3$ solution in the VFD under hydrogen gas at ambient pressure, without UV irradiation, resulted in the formation of silver particles albeit of irregular shape, as shown in Fig. S5.†

The liquid environment in the VFD promoted anisotropic crystal growth, forming bulk-like lamellar aggregates known as nanopetals. The self-assembly of these nanopetals potentially resulted in the formation of nanorods, spicules and triangles, influenced by distinct topological flows generated within the VFD thin film, as shown in Fig. 1(a)–(d). Overall, these findings

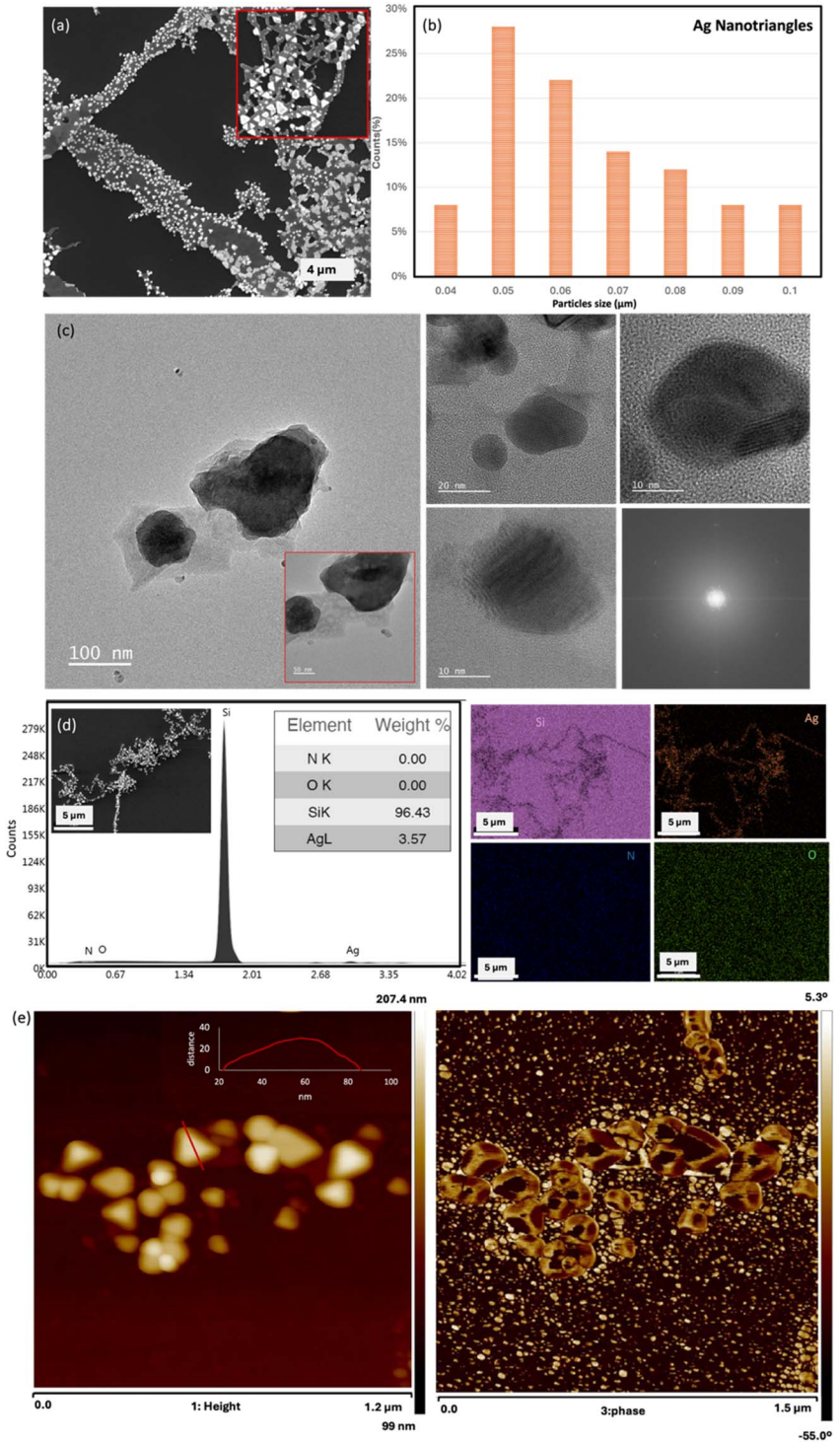

Fig. 4 (a) SEM images of Ag nanotriangles, (b) particle size distribution, (c) TEM/HRTEM image and related FFT, (d) EDX spectra and elemental mapping for Ag, N, O, and Si, and (e) AFM height profile and thickness profile for the nanotriangles. VFD processing conditions are as follows: (c) ω = 7k rpm, t = 10 min, c = 0.01 M (2 mg per mL H_2O), θ = 45°, λ = 254 nm.

highlight the effectiveness of the VFD in enabling rapid nucleation and growth of silver nanostructures, offering precise control over morphology through variation in the processing parameters. Previous mechanochemical studies on generating silver particles include the use of milling in the presence of plant extracts or lignin as natural reducing agents.[32,33] While the processing here is effective and environmentally friendly, the surfaces of the particles are not pristine. In contrast, our liquid-phase VFD method uses only water and silver nitrate, enabling *in situ* generation of hydrogen peroxide for controlled silver

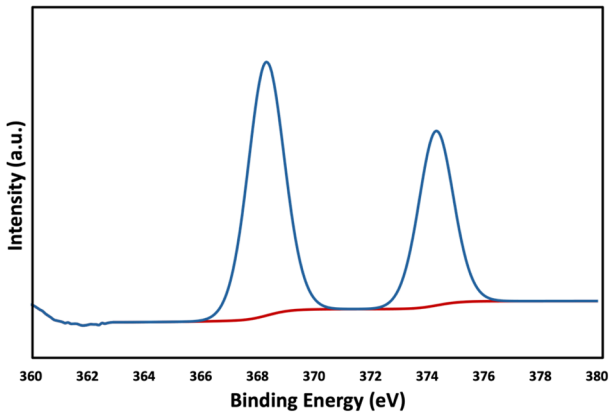

Fig. 5 XPS spectra of silver rods. The VFD processing conditions are as follows: $\omega = 5$k rpm, $t = 10$ min, $c = 0.003$ M (0.5 mg per mL H_2O), at $\theta = 45°$, $\lambda = 254$ nm.

particle synthesis with clean surfaces and tuneable morphologies. Moreover, the observed anisotropic crystal growth and self-assembly phenomena in the present work highlight the potential of the VFD for generating diverse nanostructures, which hold promise for various technological applications.

Conclusion

Following a series of experiments under confined mode conditions, we were able to optimise the formation of rod, spicule and triangle structures under continuous flow to enhance the scalability of the process. The confined mode of operation of the VFD has previously been shown to be invaluable regarding the optimization and translation of VFD processing in a continuous flow mode. In a continuous flow processing setup, a flow rate of 0.4 mL min^{-1} was used at different speeds. We established the following: (i) silver rods were formed at 5k rpm, (ii) spicule arrays at 7k rpm, and (iii) triangle structures formed at 7k rpm with an increase in concentration to 2 mg mL^{-1} of silver nitrate (0.01 M). The scaled-up production yield for materials reached approximately 80% following centrifugation for five minutes at 6900×g followed by washing with Milli-Q water.

Silver nano/micro-particles can be generated from aqueous silver nitrate solutions in the VFD under UV irradiation by the reduction of *in situ* generated reactive oxygen species, by a photo-contact electrification process. This is with control over one, two, and three-dimensional shapes, forming either rods or spicules. This rapid and efficient high yielding approach using aqueous silver nitrate affords silver particles with pristine surfaces in water in the VFD and is without the need for additional substances. Formation of the rods is presumably within the confines of the ST flow, formed where the liquid moves up through the centre of the high shear topological fluid flow, with the reactive oxygen species formed at the interface of the liquid and the quartz surface, with rapid nucleation and growth of the rods which are formed in ST flow, exiting at its top. Formation of silver spicules possibly occurs under high shear regimes when the diameter of the ST and DH flows are similar, as established for prepared spicules of fullerene C_{60}.[14] We also show that changing the concentration of the silver nitrate impacts the outcome of the nature of the resulting silver particles, which may be due to the higher ionic activity of the solution changing the nature of the topological fluid flows. Future investigations following this work will be devising methodologies for synthesizing many other nanomaterials *via* such *in situ* reduction, using water as a benign reducing agent. The utilization of the VFD process aligns with green chemistry principles by eliminating the necessity for additional substances that could contribute significantly to waste generation, while also reducing downstream processing needs.

Experimental section

Materials

Silver nitrate ($AgNO_3$, 99% purity) was purchased from Sigma-Aldrich.

Synthesis of silver nanostructures

Silver nitrate ($AgNO_3$) was diluted with Milli Q-water to reach a concentration of 0.5 mg mL^{-1} (0.003 M) or 2 mg mL^{-1} (0.01 M). Subsequently, the prepared solution (1 mL) was placed in a VFD tube 18.5 cm in length with a hemispherical base and an outer diameter (OD) of 20 mm, and the tube was then spun under ambient conditions. The tilting angle (θ) of the tube was fixed at 45°. Nanostructures were prepared from a premixed solution containing a specified volume and concentration. Subsequently 1 mL of the premixed solution was promptly transferred to the inclined VFD tube rotating at a specified rotational speed for a specified duration. A systematic evaluation of the effect of reaction time (10, 20 and 30 min), silver nitrate concentration, and rotational speed (3, 5 and 7k rpm) was conducted to establish the optimal conditions for each of the nanostructures. Two UV lamps each 10 W were positioned symmetrically on either side, aligned with the VFD tube, emitting light $\lambda = 254$ nm (lamp type-GPH212T5). For continuous flow processing, the tube was also tilted at 45° with the solution flow rate maintained at 0.4 mL min^{-1}. To remove any residual unreacted silver nitrate, the resulting samples were centrifuged (5 min, 6900×g) followed by washing with 1 mL of Milli-Q water then drop-cast onto a silicon wafer and allowed to dry in air.

Characterisation

The Ag nano/micro particles synthesised in the VFD were deposited onto a silicon substrate as a colloidal suspension in MilliQ-water through drop casting, followed by evaporation under ambient conditions. The morphology, size, and shapes of the particles were analysed using the following techniques.

Scanning electron microscopy (SEM)

SEM was conducted with an FEI F50 instrument operating at 10 kV accelerating voltage and equipped with an energy dispersive X-ray spectroscopy (EDX) facility.

Size distribution (SD)

Size distribution was measured using the Fiji distribution of Image J analysis.

Atomic force microscopy (AFM)

AFM images were acquired using a Bruker Multimode 8 AFM with a Nanoscope V controller in the tapping mode in air with all parameters including the set point, scan rate, and feedback gains adjusted to optimize the image quality. Analysis of AFM images was performed using Nanoscope analysis software version 1.4.

Transmission electron microscopy (TEM)

Analysis was carried out utilizing a JEOL JEM-F200 Multi-Purpose FEG-S/TEM system operating at 200 kV acceleration voltage. Image J software facilitated image processing tasks.

X-ray photoelectron spectroscopy (XPS)

Measurements were conducted using an instrument provided by SPECS (Berlin). A non-monochromatic X-ray source (12kV-200 W) with a Mg anode was utilized under ultra-high vacuum conditions reaching a base pressure of 10^{-10} mbar. Samples mounted on Mo sample holders on semiconductor-grade Si substrates ensured sufficient conductivity for electron compensation during exposure to X-rays, preventing any sample charging.

Data availability

The data supporting this article have been included as part of the ESI.†

Author contributions

B. A. performed all the VFD experiments and process optimization, and data analysis for SEM, SD, EDX, AFM and XPS experiments. C. L. and X. C. carried out TEM analysis. C. L. R. coordinated the research and developed the model for the fluid behaviour. The primary content of the manuscript was written by B. A., following the completion of the full draft initially by C. L. R. and other authors. All authors have given approval to the final version of the manuscript.

Conflicts of interest

There are no conflicts to declare.

Acknowledgements

The authors gratefully acknowledge the financial support from the Australia Research Council (DP200101106 and DP230100479), the technical support from the mechanical workshop teams of the College of Science, and the facilities and the scientific and technical assistance of Microscopy Australia and the Australian National Fabrication Facility (ANFF), enabled by NCRIS and the government of South Australia at Flinders Microscopy and Microanalysis, Flinders University. Engineering, Physical Sciences Building, Flinders University.

References

1 S. H. Lee and B.-H. Jun, Silver nanoparticles: synthesis and application for nanomedicine, *Int. J. Mol. Sci.*, 2019, **20**(4), 865.
2 X.-F. Zhang, *et al.*, Silver nanoparticles: synthesis, characterization, properties, applications, and therapeutic approaches, *Int. J. Mol. Sci.*, 2016, **17**(9), 1534.
3 H. D. Beyene, *et al.*, Synthesis paradigm and applications of silver nanoparticles (AgNPs), a review, *Sustainable Mater. Technol.*, 2017, **13**, 18–23.
4 P. M. Gopinath, *et al.*, Mycosynthesis, characterization and antibacterial properties of AgNPs against multidrug resistant (MDR) bacterial pathogens of female infertility cases, *Asian J. Pharm. Sci.*, 2015, **10**(2), 138–145.
5 A. Baran, *et al.*, Investigation of antimicrobial and cytotoxic properties and specification of silver nanoparticles (AgNPs) derived from Cicer arietinum L. green leaf extract, *Front. Bioeng. Biotechnol.*, 2022, **10**, 855136.
6 J. Helmlinger, *et al.*, Silver nanoparticles with different size and shape: equal cytotoxicity, but different antibacterial effects, *RSC Adv.*, 2016, **6**(22), 18490–18501.
7 B. Khodashenas and H. R. Ghorbani, Synthesis of silver nanoparticles with different shapes, *Arabian J. Chem.*, 2019, **12**(8), 1823–1838.
8 A. A. Yaqoob, K. Umar and M. N. M. Ibrahim, Silver nanoparticles: various methods of synthesis, size affecting factors and their potential applications–a review, *Appl. Nanosci.*, 2020, **10**(5), 1369–1378.
9 S. Zeroual, *et al.*, Ethylene glycol based silver nanoparticles synthesized by polyol process: Characterization and thermophysical profile, *J. Mol. Liq.*, 2020, **310**, 113229.
10 L. Marciniak, *et al.*, The effect of pH on the size of silver nanoparticles obtained in the reduction reaction with citric and malic acids, *Materials*, 2020, **13**(23), 5444.
11 E. Hermosilla, *et al.*, Molecular weight identification of compounds involved in the fungal synthesis of AgNPs: Effect on antimicrobial and photocatalytic activity, *Antibiotics*, 2022, **11**(5), 622.
12 R. Razavi, *et al.*, Green synthesis of Ag nanoparticles in oil-in-water nano-emulsion and evaluation of their antibacterial and cytotoxic properties as well as molecular docking, *Arabian J. Chem.*, 2021, **14**(9), 103323.
13 P. Puprompan, *et al.*, Flow synthesis of silver nanoparticles using water in supercritical CO2 emulsion, *J. CO2 Util.*, 2024, **83**, 102776.
14 T. M. Alharbi, *et al.*, Sub-micron moulding topological mass transport regimes in angled vortex fluidic flow, *Nanoscale Adv.*, 2021, **3**(11), 3064–3075.
15 T. M. D. Alharbi, *et al.*, Controlled slicing of single walled carbon nanotubes under continuous flow, *Carbon (New York)*, 2018, **140**, 428–432.

16 A. H. M. Al-Antaki, *et al.*, Inverted vortex fluidic exfoliation and scrolling of hexagonal-boron nitride, *RSC Adv.*, 2019, **9**(38), 22074–22079.
17 T. M. Alharbi, *et al.*, Shear stress mediated scrolling of graphene oxide, *Carbon*, 2018, **137**, 419–424.
18 K. Vimalanathan, *et al.*, Vortex fluidic mediated transformation of graphite into highly conducting graphene scrolls, *Nanoscale Adv.*, 2019, **1**(7), 2495–2501.
19 X. Luo, *et al.*, Laser irradiated vortex fluidic mediated synthesis of luminescent carbon nanodots under continuous flow, *React. Chem. Eng.*, 2018, **3**(2), 164–170.
20 K. Vimalanathan, *et al.*, Surfactant-free Fabrication of Fullerene C60 Nanotubules Under Shear, *Angew. Chem.*, 2017, **129**(29), 8518–8521.
21 F. A. Alrashaidi, *et al.*, Vortex Mediated Fabrication of 2D Antimonene Sheets From Antimony Powder, *RSC Mechanochem.*, 2024, **1**, 432–436.
22 J. Britton, *et al.*, Accelerating enzymatic catalysis using vortex fluidics, *Angew. Chem., Int. Ed.*, 2016, **55**(38), 11387–11391.
23 L. Yasmin, *et al.*, Optimising a vortex fluidic device for controlling chemical reactivity and selectivity, *Sci. Rep.*, 2013, **3**(1), 2282.
24 T. Z. Yuan, *et al.*, Shear-stress-mediated refolding of proteins from aggregates and inclusion bodies, *ChemBioChem*, 2015, **16**(3), 393–396.
25 M. Jellicoe, *et al.*, Vortex fluidic induced mass transfer across immiscible phases, *Chem. Sci.*, 2022, **13**(12), 3375–3385.
26 C. Chuah, *et al.*, Thin-film flow technology in controlling the organization of materials and their properties: Special Collection: Distinguished Australian Researchers, *Aggregate*, 2024, **5**(1), e433.
27 B. M. Alotaibi, *et al.*, Nanogold Foundry Involving High-Shear-Mediated Photocontact Electrification in Water, *Small Sci.*, 2024, 2300312.
28 J. Britton, *et al.*, Vortex fluidic chemical transformations, *Chem. – Eur. J.*, 2017, **23**(54), 13270–13278.
29 P. R. Gogate, R. K. Tayal and A. B. Pandit, Cavitation: a technology on the horizon, *Curr. Sci.*, 2006, 35–46.
30 A. Vasil'kov, *et al.*, XPS study of silver and copper nanoparticles demonstrated selective anticancer, proapoptotic, and antibacterial properties, *Surf. Interface Anal.*, 2022, **54**(3), 189–202.
31 T. Parnklang, *et al.*, Shape transformation of silver nanospheres to silver nanoplates induced by redox reaction of hydrogen peroxide, *Mater. Chem. Phys.*, 2015, **153**, 127–134.
32 M. Baláž, *et al.*, Mechanochemistry as an alternative method of green synthesis of silver nanoparticles with antibacterial activity: A comparative study, *Nanomaterials*, 2021, **11**(5), 1139.
33 M. J. Rak, T. Friščić and A. Moores, One-step, solvent-free mechanosynthesis of silver nanoparticle-infused lignin composites for use as highly active multidrug resistant antibacterial filters, *RSC Adv.*, 2016, **6**(63), 58365–58370.